Development and preclinical evaluation of [18F]FBVM as a new potent PET tracer for vesicular acetylcholine transporter

Johnny Vercouillie, Frédéric Buron, Sophie Sérrière, Nuno Rodrigues, Zuhal Gulhan, Agnès Chartier, Gabrielle Chicheri, Hamid Marzag, Adeline Oury, Nathalie Percina, et al.

Development and preclinical evaluation of [^{18}F]FBVM as a new potent PET tracer for vesicular acetylcholine transporter

Johnny Vercouillie[a1], Frédéric Buron[b1], Sophie Sérrière[a1], Nuno Rodrigues[b], Zuhal Gulhan[a], Agnès Chartier[b], Gabrielle Chicheri, [a] Hamid Marzag[b], Adeline Oury[a], Nathalie Percina[b], Sylvie Bodard[a], Rajah Ben Othman[b], JulieBusson[a], Franck Suzenet[b], Denis Guilloteau[a], Mathieu Marchivie[c], Patrick Emond[a], Sylvain Routier[b1*], [1]Sylvie Chalon[a1*]

[a] *UMR 1253, iBrain, Université de Tours, Inserm, Tours, France*
[b] *ICOA, UMR CNRS 7311, Université d'Orléans, Orléans, France*
[c] *Univ. Bordeaux, CNRS, Bordeaux INP, ICMCB, UMR 5026, F-33600, Pessac, France*

* Corresponding author. *E-mail addresses:* sylvain.routier@univ-orleans.fr (S. Routier), sylvie.chalon@univ-tours.fr (S. Chalon).
1 These authors contributed equally.

Abstract

Age-related neurodegenerative diseases have in common the occurrence of cognitive impairment, a highly incapacitating process that involves the cholinergic neurotransmission system. The vesicular acetylcholine transporter (VAChT) positron emission tomography (PET) tracer [^{18}F]fluoroethoxybenzovesamicol ((−)-[^{18}F]FEOBV) has recently demonstrated its high value to detect alterations of the cholinergic system in Alzheimer's disease, Parkinson's disease and dementia with Lewy body. We present here the development of the new vesamicol derivative tracer (−)-(R,R)-5-[^{18}F]fluorobenzovesamicol ((−)[^{18}F]FBVM) that we compared to (−)[^{18}F]FEOBV in the same experimental conditions. We show that: i) *in vitro* affinity for the VAChT was 50-fold higher for (−)FBVM (Ki = 0.9 ± 0.3 nM) than for (−)FEOBV (Ki = 61 ± 2.8 nM); ii) *in vivo* in rats, a higher signal-to-noise specific brain uptake and a lower binding to plasma proteins and peripheral defluorination were obtained for (−)[^{18}F]FBVM compared to (−)[^{18}F]FEOBV. Our findings demonstrate that (−)[^{18}F]FBVM is a highly promising PET imaging tracer which could be sufficiently sensitive to detect in humans the cholinergic denervation that occurs in brain areas having a low density of VAChT such as the cortex and hippocampus.

Keywords : Alzheimer's disease, Neuroimaging, Parkinson's disease, Radiopharmaceutical, Vesamicol

1. Introduction

Age-related neurodegenerative diseases such as Alzheimer's disease (AD), Parkinson's disease (PD) and different types of dementia including Parkinson's disease dementia (PDD) and dementia with Lewy body (DLB) are a growing public health problem [1]. These diseases are complex and heterogeneous, involving the dysfunction of several distinct neuronal networks [2], and to date no curative treatment is available. Therefore, a major challenge that could improve treatments would be to differentiate sub-phenotypes during the disease course and ideally from the early stages. In this context, positron emission tomography (PET) imaging is unquestionably a highly relevant tool. This method can localize and quantify longitudinally with high sensitivity various brain molecular targets able to reflect either broad mechanisms such as mitochondrial and synaptic dysfunctions and neuroinflammation, or more specific hallmarks such as abnormal protein aggregates and neurotransmission system alterations [3].

These neurodegenerative diseases have in common the occurrence of cognitive impairment, a highly incapacitating process that involves various actors among which the cholinergic neurotransmission system [4-6]. The involvement of this system can be monitored through PET neuroimaging of different molecular targets, both at pre-synaptic and post-synaptic level. Regarding the post-synaptic acetylcholine receptors, several clinical studies have described a reduction in the nicotinic α4β2 subtype in AD [7-10] and PD [11-13]. At the pre-synaptic level, the brain uptake of radiolabelled substrates of acetylcholinesterase has been shown to decrease in several neurodegenerative disorders associated to cognitive deficits [14-17]. Another pre-synaptic marker, i.e. the vesicular acetylcholine transporter (VAChT) had already been shown to be reduced using the SPECT tracer [^{123}I]iodobenzovesamicol, [^{123}I]IBVM in several neurodegenerative disorders [18-20] and a new interest of this index of cognitive impairment recently emerged in studies demonstrating that the VAChT PET tracer [^{18}F]fluoroethoxybenzovesamicol ([^{18}F]FEOBV) described in 1998 [21] is of great value in detecting alterations of the cholinergic system in AD [22-24], PD [25,26], and DLB [27,28].

The organisation of the cholinergic system is highly complex and diffuse, with cell bodies localised in different brain structures such as the basal forebrain and brainstem, in the form of groups projecting into specific target areas such as the hippocampus, olfactory bulbs, amygdala, neocortex, and thalamus [29,30]. The case of striatal cholinergic interneurons is particular, with limited localisation in the structure. The VAChT, which is responsible for the storage of acetylcholine in synaptic vesicles [31], is present both in cell bodies and neuron endings [32]. PET exploration of the VAChT can therefore be highly informative regarding the integrity of cholinergic neurons, on condition that this method displays a sufficiently high resolution and sensitivity to detect and quantify low densities of this molecular target in small brain areas. This requires that the radioactive probe should have especially a high affinity for the target [33].

By comparison with the available tracer (−)-FEOBV, (−)-5-fluorobenzovesamicol ((−)-FBVM) was previously found to have a more than 5 times higher affinity for the VAChT [34] (Fig. 1). We therefore hypothesised that its radioactive analogue could be a powerful PET imaging tool. We present here the synthesis and characterization of the racemic and enantiopure 5-FBVM derivatives which were then radiolabeled with fluor-18, purified, and compared *in vivo* to (−)-[^{18}F]FEOBV in the rat.

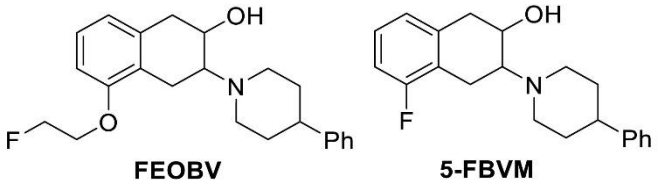

Fig. 1. FEOBV and FBVM

2. Results and discussion

2.1. Chemistry and radiochemistry

From our previous study [34], we demonstrated the high affinity of FBVM enantiomers to bind to VAChT (around 4 nM for the (−)-FBVM). In a first attempt to radiolabel these compounds with fluorine-18 we used fluoro-de-triazenation, but unfortunately this approach did not lead to the expected radiolabelled compounds. In the last decade, significant improvements in S_NAr fluorine-18 radiolabelling were achieved even on a deactivated position [35-37]. Thus, after having successfully obtained a radiofluorinated COX-2 compound with a fluorine on the aromatic ring, we focused our radiolabelling strategy on the use of a pinacol borane precursor [38]. For the cold chemistry, we first focused our efforts on the synthesis of racemic 5-aminobenzovesamicol **2** in a large scale (multigram) from 1-aminonaphthalene **1** [39]. Preparation of **3** was achieved under a revised Balz-Schiemann procedure involving the use of *tert*-butyl nitrite and BF_3•Et_2O and PIDA as reagents [40]. This synthesis approach led to trans isomers and a chiral separation on Chiralpak IA led to the 2 pure stereoisomers **6** and **7** (retention time: 16 min and 21 min, respectively) in a near 50/50 ratio but at this step, no indication of the absolute configuration of each asymmetric carbon was available (Scheme 1).

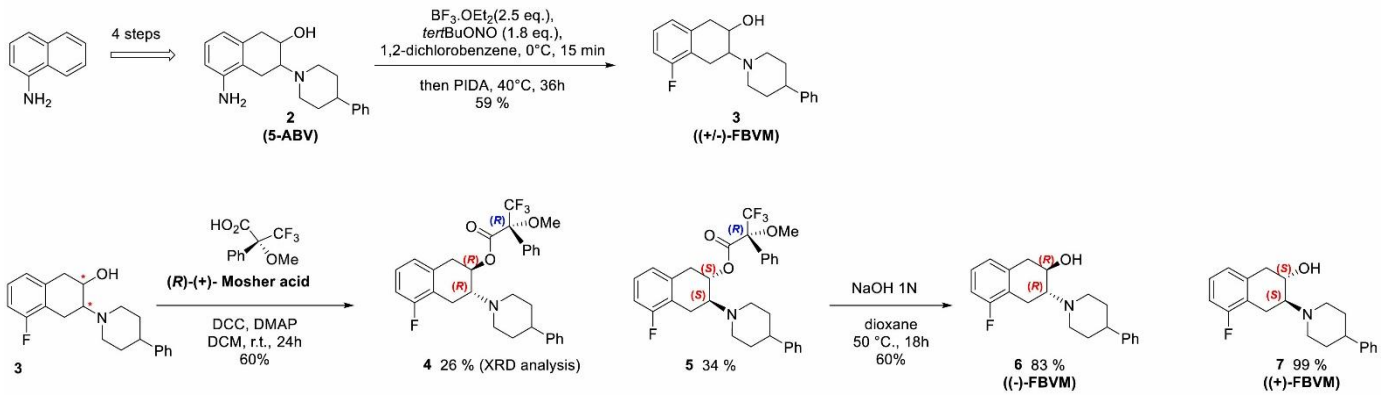

*Scheme 1. Synthesis of FBVM isomers and chiral Mosher diasteroisomers **4/5**.*

To determine formally the absolute configuration of each asymmetric carbon, we used the Mosher derivatization method. **3** and (*R*)-Mosher's acid under Steglich esterification led to the two diastereoisomer esters **4** and **5** which were easily separated by flash chromatography. The hydrochloride form of **4** was crystalized and gave single crystals suitable for X-ray diffraction analysis. **4** crystallizes in the non-centrosymmetric orthorhombic space group $P2_12_12_1$ (Table S1, supporting information). The asymmetric unit contains one protonated molecule and a chloride anion (Fig. 1). The bond lengths are all in the expected range (1.369(10) – 1.405(8) for the C–C bonds of aromatic rings, 1.501(7) – 1.546(6) for C–C or C–N single bonds, 1.325(7) – 1.355(6) for C–F bonds, 1.439(8) – 1.462(6) for C–O single bonds and 1.214(6) and 1.329(6) for the carboxyl group corresponding respectively to the C=O double bond and C–O single bond with a partially delocalised doublet), aromatic rings are almost planar (max deviation: 0.008 Å for C4) and cyclohexane and piperidine moieties present the boat and chair conformation respectively. The cohesion of the network is ensured by charge assisted H-bonding between the ammonium group and the chloride anion, completed by weaker van der Waals interactions.

The absolute configuration of the crystal structure was assigned by analysis of the Bijvoet differences leading to a Hooft parameter of 0.00(2) and a Flack parameter of 0.02(2) [41-43]. According to these two parameters, both significantly very close to zero, it can be formally established that the three asymmetric carbons possess R absolute configurations. An ORTEP representation of the molecular structure is given in Fig. 2. To our knowledge, this is the first crystallization of a vesamicol derivative leading to a formal identification of asymmetric centres as well as the confirmation of the 3D relative conformation of each element of the pharmacophore.

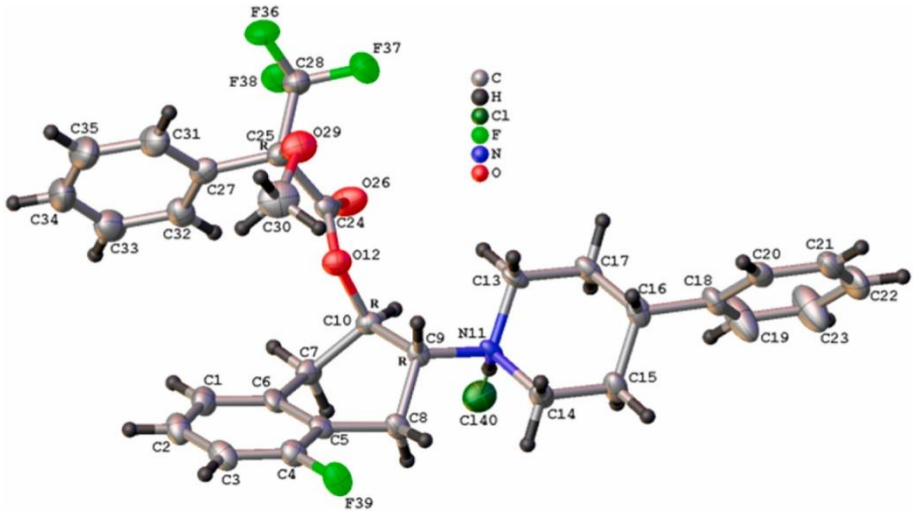

*Fig. 2. ORTEP representation of the asymmetric unit of **4•HCl** and identification of the R,R,R absolute configurations of chiral carbons (C9, C10 and C25). The thermal ellipsoids are drawn at the 50% probability level.*

In order to verify concordance between all the results, a saponification of **4** was performed and led to **6** which co-eluted under our HPLC conditions with **(–)-FBVM** and corresponded to the first peak observed after **(*rac*)-FBVM** chiral HPLC

analysis**.** Finally, saponification of **5** led to the enantiopure **7** which co-eluted with **(+)-FBVM** and the second peak observed after **(*rac*)-FBVM** chiral HPLC analysis.

The compound **2** led first to **8** after diazotation and reaction with KI in moderate yield (Scheme 2). A palladium catalysed reaction involving Pd(dppf)Cl_2 as catalyst and Bis(pinacolato)diboron led to the boronic ester **9** which was used to perform radiolabelling with radiofluoride ion. The low yield obtained for **7** is due to difficulties of purifying the boronic ester. The racemic [^{18}F]**10** was obtained using Cu(OTf)$_2$ as catalyst, with pyridine in DMF followed by HPLC purification on a reverse phase column. An additional HPLC purification using a Chiralpak IA chromatography column (Fig. 3A) led to the two corresponding enantiopure probes **11** ((−)-(*R,R*)) and **12** ((+)-(*S,S*)) by order of elution (Fig. 3B).

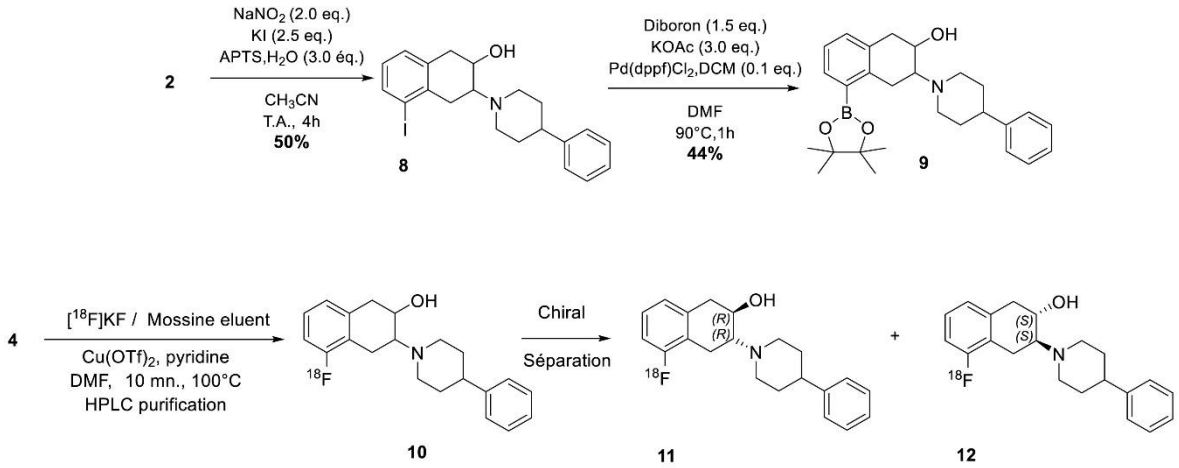

*Scheme 2. Synthesis of precursor **9** and its radiolabeling with ^{18}F up to chiral purification to get pure **11 (−)**-(R,R) or **12 (+)**- (S,S).*

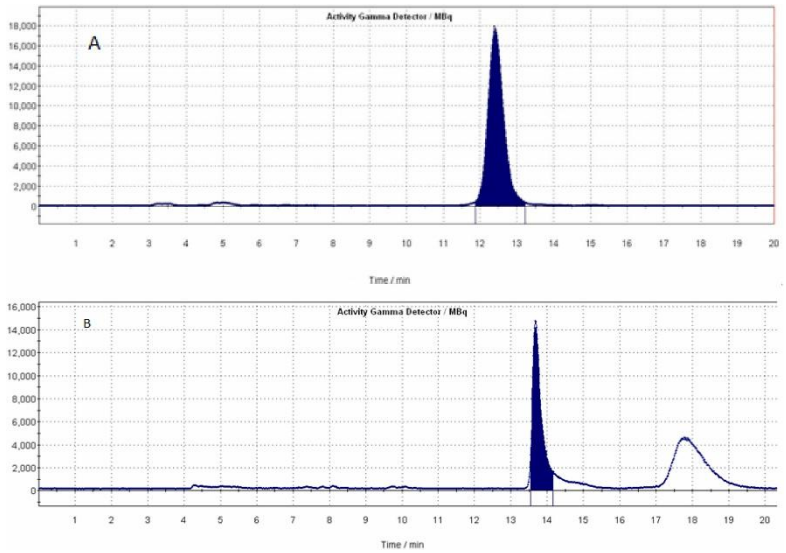

*Fig. 3. Semi-preparative purification to obtain **10** (rac), **11** (−)-(R,R) or **12** (+)-(S,S). Only radioactive signals are reported: A) Purification on Luna PhenylHexyl to obtain **10**; B) Purification on Chriralpak IA to obtain **11** or **12** with time retention of 13.7 and 17.8 min, respectively.*

The whole process leading to **10** *(rac)* was achieved in 60 ± 2 min with a radiochemical yield (RCY) up to 43% and a molar activity between 75 and 151 GBq/µmole. The production of **11** and **12** was achieved in 83 and 87 min, respectively, with a RCY up to 29% and molar activity in the 70–145 GBq/µmole range.

The (−)-[^{18}F]FEOBV was synthesized using a method adapted from the original process described by Mulholland et al. [44]. The pure precursor (−)-TEBV was heated at 115 °C for 7.5 min, then the reaction was cooled and quenched with water. The following steps were similar to the process used for (+/−)-[^{18}F]FBVM production. The radiosynthesis of (−)-[^{18}F]FEOBV was achieved in 80 ± 3 min with a RCY of 71 ± 10.1% and a molar activity of 248.9 ± 56.4 GBq/µmole.

The chemical and plasmatic stability of **10** were checked up to 4h after the end of production and no degradation of the probe was observed.

2.2. In vitro experiments

The affinity properties for the VAChT and the enantioselectivity of new blocking agents derived from vesamicol were first described in an extensive structure-activity study that demonstrated the high potency of the chemical family of benzovesamicol [45]. At that time, the growing interest in imaging *in vivo* the VAChT as a relevant marker of cholinergic terminals led to several of these compounds such as [^{123}I]IBVM [46] and [^{18}F]FEOBV [21] being radiolabelled. In the present study, we achieved the synthesis and formal identification of pure FBVM **3** (*Rac*), **6** (−)-FBVM and **7** (+)-FBVM. This allowed us to measure the affinity of these compounds in comparison to the (+/−)-FEOBV and (−)-FEOBV enantiomer in the same *in vitro* experiments performed on a rat brain membrane preparation, in order to confront the results to those obtained in *in vivo* studies using the fluor-18-labelled derivatives. As shown in Table 1, the affinity for the VAChT of the **3** (*Rac*) was excellent (Ki = 1.3 ± 0.2 nM towards the reference probe [^{3}H]vesamicol), slightly better for the **6** (−)-FBVM enantiomer (Ki = 0.9 ± 0.3 nM), and indisputably lower for the **7** (+)-FBVM enantiomer (Ki = 35 ± 5 nM). In comparison to our FBVM compounds, the affinity of the (+/−)-FEOBV and (−)-FEOBV enantiomer was 40- to 50-fold reduced (Ki = 61 ± 2.8 nM and 50 ± 10 nM, respectively). These results agreed with the enantioselectivity of vesamicol derivatives, although we found for the FBVM compounds a better *in vitro* affinity for the VAChT than that previously published (Ki = 3.68, 6.95 and 10.9 nM for the (−) enantiomer, (+) enantiomer and rac, respectively), in different experimental conditions, i.e. cell extracts expressing the rat VAChT [34] instead of rat fresh tissue in our studies. However, it is noticeable that in both studies, the FBVM compounds had a better affinity than the FEOBV compounds, e.g., 50-fold for the (−) enantiomers in the present study (Table 1).

Table 1
Affinity for the VAChT of FBVM and FEOBV racemic and enantiomers.

	Ki (nM)
(+/−)-FBVM **3**	1.3 ± 0.2
(−)-FBVM **6**	0.9 ± 0.3
(+)-FBVM **7**	35 ± 5
(+/−)-FEOBV	61 ± 2.8
(−)-FEOBV	50 ± 10

The Ki towards VAChT was measured on a membrane preparation from rat brain hemispheres according to a modified version of a previously described method [47] using [^{3}H]vesamicol. The IC_{50} values were determined graphically for each compound and the Ki was calculated according to Cheng and Prussof [48]. The results are expressed as mean Ki ± SEM from 3 independent experiments.

2.3. Ex vivo biodistribution and *in vivo* PET imaging in the rat brain

To date, (−)-[^{18}F]FEOBV is the best characterized PET tracer useful for VAChT imaging in animal models [21,49-53] and humans, in physiological [54] and more recently pathological [55-61] conditions. Therefore, we compared our new FBVM compounds to this reference tracer in the rat model by performing *ex vivo* biodistribution experiments and *in vivo* PET imaging.

The accumulation of (+/−)-[^{18}F]FBVM **10**, (−)-[^{18}F]FBVM **11**, (+)-[^{18}F]FBVM **12** and (−)-[^{18}F]FEOBV was then studied at 2 h after i.v. injection in animals that received (Vesamicol groups) or not (Control groups) a pre-injection of the VAChT antagonist vesamicol.

In the control group receiving (−)-[^{18}F]FEOBV, we observed a blood level accumulation of 0.265 ± 0.09% ID/g, in agreement with previously published data [21], whereas it was significantly lower for (+/−)-[^{18}F]FBVM **10**, (+)-[^{18}F]FBVM **12** and (−)-[^{18}F]FBVM **11** (0.016 ± 0.001, 0.016 ± 0.001 and 0.012 ± 0.001% ID/g, respectively). The bone accumulation, which is an index of *in vivo* defluorination, was also higher for (−)-[^{18}F]FEOBV (0.254 ± 0.011% ID/g) than for FBVM derivatives (0.108 ± 0.05, 0.105 ± 0.007 and 0.096 ± 0.06% ID/g for (+/−)-[^{18}F]FBVM **10**, (+)-[^{18}F]FBVM **12** and (−)-[^{18}F]FBVM **11**, respectively). Overall, these results can be explained by a higher binding to plasma proteins and a higher peripheral radio-defluorination for (−)-[^{18}F]FEOBV than for the [^{18}F]FBVM racemic and enantiomers, which could reduce the free plasmatic fraction available for brain uptake.

In the brain (Table 2), the uptake of (+/−)-[^{18}F]FBVM **10**, (−)-[^{18}F]FBVM **11** and (−)-[^{18}F]FEOBV in control groups was significantly higher in the striatum and significantly lower in the cerebellum than in other brain regions (i.e., the frontal cortex, hippocampus and thalamus). However, for (+)-[^{18}F]FBVM **12**, a statistically significant difference was reached exclusively between the striatum and cerebellum.

Table 2
Brain biodistribution of (+/−)-[^{18}F]FBVM 10, (+)-[^{18}F]FBVM 12, (−)-[^{18}F]FBVM 11, and (−)-[^{18}F]FEOBV in control and vesamicol-injected rats.

	(+/−)-[^{18}F]FBVM 10		(+)-[^{18}F]FBVM 12		(−)-[^{18}F]FBVM 11		(−)-[^{18}F]FEOBV	
	Control (n = 6)	VES (n = 6)	Control (n = 6)	VES (n = 5)	Control (n = 8)	VES (n = 9)	Control (n = 6)	VES (n = 6)
Cer	0.185 ±0.003	0.062 ±0.003**	0.215 ±0.011	0.057 ±0.004**	0.232 ±0.017	0.095 ±0.008*	0.235 ±0.011	0.235 ±0.010
Stri	0.721 ±0.011††	0.379 ±0.015**	0.327 ±0.015†	0.105 ±0.009**	1.356 ±0.069††	0.736 ±0.045**	0.844 ±0.025††	0.594 ±0.030**
Cx	0.420 ±0.005††	0.166 ±0.009**	0.265 ±0.012	0.075 ±0.006**	0.723 ±0.052††	0.333 ±0.023**	0.450 ±0.013††	0.347 ±0.016**
Hip	0.402 ±0.008††	0.153 ±0.007**	0.296 ±0.011	0.073 ±0.007**	0.611 ±0.041††	0.349 ±0.045**	0.382 ±0.011†	0.326 ±0.014
Thal	0.368 ±0.005††	0.157 ±0.006**	0.258 ±0.014	0.084 ±0.007**	0.591 ±0.032††	0.312 ±0.018**	0.468 ±0.018††	0.370 ±0.018*

All rats were sacrificed at 2 h after i.v. injection of the tracer. In the vesamicol-injected groups (VES), animals received an i.v. injection of (−)vesamicol at the dose of 0.5 µmol/kg, 5 min before tracer injection. The results are expressed as mean % injected dose/g tissue ± SEM in different rat brain regions, i.e., the cerebellum (Cer), striatum (Stri), frontal cortex (Cx), hippocampus (Hip), and thalamus (Thal).

Values were compared using the two-way Anova, Bonferroni post-hoc test. In Control groups: †$p < 0.01$, ††$p < 0.001$ *vs* cerebellum. In VES groups: *$p < 0.01$, **$p < 0.001$ *vs* Control group in the same brain region.

A striatum-to-cerebellum uptake ratio of 3.90, 1.52, 5.84 and 3.59 was obtained for (+/−)-[^{18}F]FBVM **10**, (+)-[^{18}F]FBVM **12**, (−)-[^{18}F]FBVM **11** and (−)-[^{18}F]FEOBV, respectively. The comparison of the ratio between the extra-striatal areas, i.e., the frontal cortex, hippocampus, thalamus, and the cerebellum showed that it was always higher for (−)-[^{18}F]FBVM **11** (3.12, 2.63, 2.55, respectively) than for (−)-[^{18}F]FEOBV (1.91, 1.63, 1.99).

The PET images of each tracer recorded between 1 and 2 h post-injection were in perfect agreement with the above *ex vivo* biodistribution study in control animals, illustrating that a clearly higher signal-to-noise ratio was obtained for (−)-[^{18}F]FBVM **11** compared to the other tracers, whereas a poorly contrasted image was obtained for (+)-[^{18}F]FBVM **12** (Fig. 4).

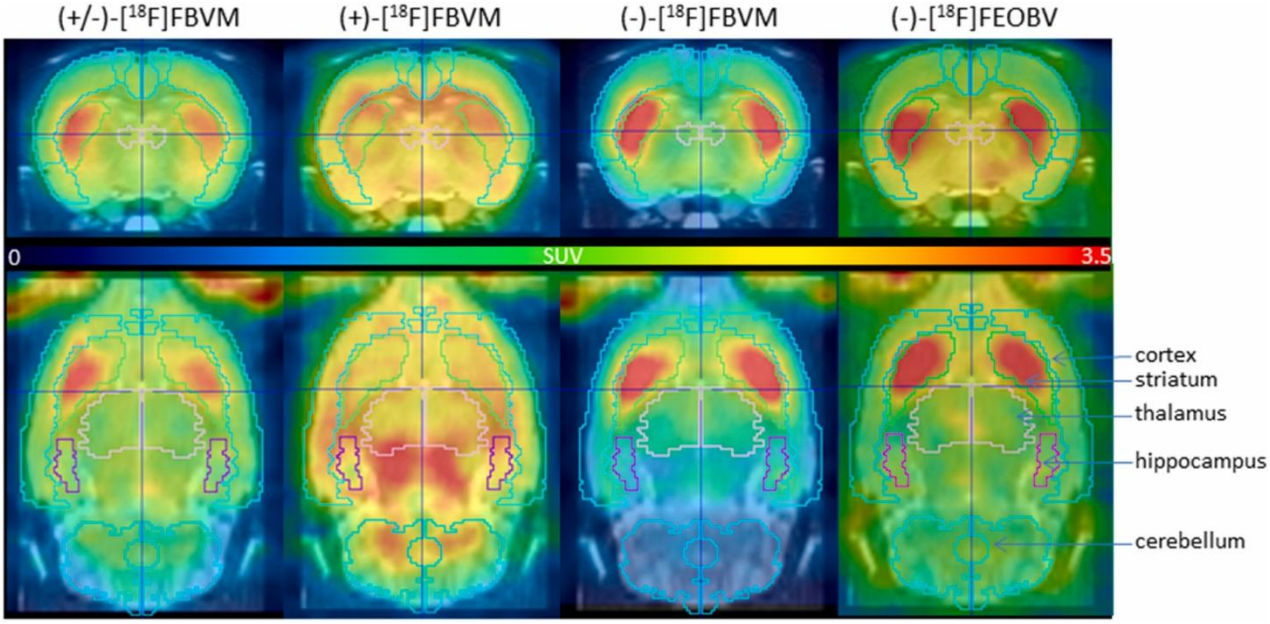

*Fig. 4. PET studies in rat brain. Representative (+/−)-[^{18}F]FBVM **10**, (+)-[^{18}F]FBVM **12**, (−)-[^{18}F]FBVM **11** and (−)-[^{18}F]FEOBV images, 60–120 min p.i. Top: coronal view, bottom: horizontal view.*

Overall, both *ex vivo* biodistribution and *in vivo* imaging in control rats showed that the regional brain distribution of (+/−)-[^{18}F]FBVM **10**, (−)-[^{18}F]FBVM **11** and (−)-[^{18}F]FEOBV was in agreement with the known localisation of the VAChT which is considered as an index of cholinergic innervation and can be explored by nuclear imaging methods using the cerebellum as a brain region of non-specific binding [21,46].

We also compared the *in vivo* kinetics of our best vesamicol derivatives (−)-[^{18}F]FBVM **11** and (−)-[^{18}F]FEOBV, and observed that both tracers had a rapid accumulation in the brain and then a progressive washout with a plateau between 60 and 120 min post-injection (Fig. 5), in agreement with previously reported data with [^{18}F]FEOBV in rodent brain [21,52].

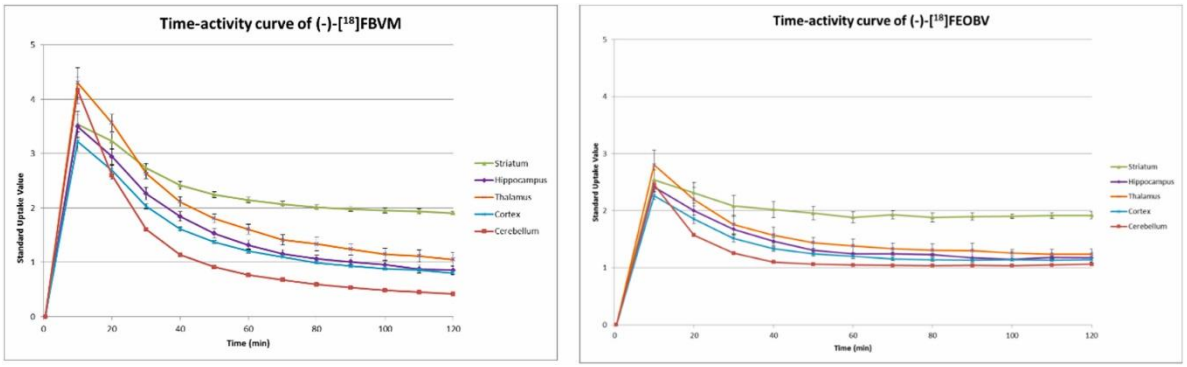

*Fig. 5. Time-activity curves of (−)-[^{18}F]FBVM **11** (n = 4) and (−)-[^{18}F]FEOBV (n = 2) in different brain regions.*

Our *ex vivo* competition experiments (i.e., VES groups) demonstrated that in agreement with their brain localisation in control groups, the uptake of the 4 tracers was mainly related to their binding to the VAChT. The pre-administration of vesamicol induced a significant decrease of radioactivity in the striatum (−47%, −68%, −46% and −30% for (+/−)-[^{18}F]FBVM **10**, (+)-[^{18}F]FBVM **12**, (−)-[^{18}F]FBVM **11** and (−)-[^{18}F]FEOBV in comparison to control groups, respectively; Table 2). The uptake was also significantly reduced in other brain regions than the striatum in VES groups except for (−)-[^{18}F]FEOBV in the cerebellum and hippocampus. The fact that the vesamicol pre-injection induced a reduction of (+/−)-[^{18}F]FBVM **10**, (+)-[^{18}F]FBVM **12**, and (−)-[^{18}F]FBVM **11** but not (−)-[^{18}F]FEOBV uptake in the cerebellum which has very poor cholinergic innervation, could be related to an *in vivo* binding of the FBVM compounds on other sites than the VAChT. This characteristic had previously been observed for several imaging tracers with a benzovesamicol structure [62].

In order to look deeper into this point, we performed an *ex vivo* competition experiment comparing our best new tracer (−)-[^{18}F]FBVM **11** with (−)-[^{18}F]FEOBV using a pre-injection of haloperidol which is known to be a potent antagonist of

dopamine D2 and also sigma receptors [63]. As observed in control groups from the previous experiment, the uptake of (−)-[^{18}F]FBVM **11** and (−)-[^{18}F]FEOBV was significantly lower in the cerebellum than in the other brain regions studied (Table 3). In these groups, we also obtained similar striatum-to-cerebellum uptake ratios to previously, with values of 5.98 and 3.94 for (−)-[^{18}F]FBVM **11** and (−)-[^{18}F]FEOBV, respectively.

Table 3
Brain biodistribution of **(−) [^{18}F] FBVM 11** and **(−) [^{18}F] FEOBV** in control and haloperidol-injected rats.

	(−)[^{18}F]FBVM 11		(−)[^{18}F]FEOBV	
	Control (n = 6)	HAL (n = 6)	Control (n = 6)	HAL (n = 6)
Cer	0.197 ±0.003	0.067 ±0.003*	0.269 ±0.009	0.248 ±0.006
Stri	1.178 ±0.046††	1.714 ±0.042**	1.06 ±0.061††	1.586 ±0.063**
Cx	0.512 ±0.023††	0.358 ± 0.01**	0.581 ±0.012††	0.504 ±0.025
Hip	0.444 ±0.019††	0.418 ± 0.03	0.486 ±0.012††	0.479 ±0.02
Thal	0.478 ±0.02††	0.353 ± 0.013*	0.484 ±0.013††	0.441 ±0.019

All rats were sacrificed at 2 h after i.v. injection of the tracer. In the Haloperidol groups (HAL), animals received an i.v. injection of haloperidol at the dose of 1 mg/kg (2.6 µmol/kg), 5 min before tracer injection.

Results are expressed as mean % injected dose/g tissue ± SEM in different rat brain regions, i.e., the cerebellum (Cer), striatum (Stri), frontal cortex (Cx), hippocampus (Hip), and thalamus (Thal).

Values were compared using the two-way Anova, Bonferroni post-hoc test. In Control groups: †$p < 0.01$, ††$p < 0.001$ *vs* cerebellum. In HAL groups: *$p < 0.01$, **$p < 0.001$ *vs* Control group in the same brain region.

We observed that the administration of haloperidol had no effect on the blood level of the two tracers at 2 h post-injection, with values similar to those obtained in the previous experiment ((−)-[^{18}F]FBVM **11**: 0.011 ± 0.001 and 0.013 ± 0.001%ID/g in the HAL and control group, respectively; (−)-[^{18}F]FEOBV: 0.274 ± 0.007 and 0.284 ± 0.01%ID/g in the HAL and control group, respectively). In contrast, it had previously been shown that the pre-injection of haloperidol was able to induce a reduction in blood activity and overall brain uptake of (−)-[^{18}F]FEOBV in mice, but the dose was 10-fold higher than in the present study [21]. Our experiment also showed a rise in the uptake of both (−)-[^{18}F]FBVM **11** (+46%) and (−)-[^{18}F]FEOBV (+50%) specifically in the striatum of HAL groups compared to controls, as already observed in the above-mentioned study [21]. Such a result had also been observed with other tracers from the benzovesamicol chemical family and was related to the increased cholinergic activity induced by the blockage of dopamine D2 receptors by haloperidol [64,65]. The haloperidol pre-injection induced a significant reduction in the uptake of (−)-[^{18}F]FBVM **11** in brain regions other than the striatum, i.e., the cerebellum (−66%), frontal cortex (−30%) and thalamus (−26%), whereas no modification was detected for (−)-[^{18}F]FEOBV (Table 3). Such a reduction had already been observed with other benzovesamicol VAChT tracers [65] and could be related to the blockade of σ receptors which are almost homogeneously localized in the rat brain with a lower expression in the striatum [66]. A reduced influx rate of (−)-[^{18}F]FEOBV was also observed in the same brain regions with a high dose of haloperidol (10 mg/kg) [52]. Overall, our comparison study could be related to a potential higher *in vivo* binding of (−)-[^{18}F]FBVM **11** than (−)-[^{18}F]FEOBV to σ receptors.

3. Conclusions

We have described for the first time a new PET tracer useful for VAChT imaging, (−)-[^{18}F]FBVM **11**, and identified the absolute configuration of its chemical structure. We demonstrated the major importance of enantiomerism, with a highly improved *in vitro* affinity and *in vivo* signal-to-noise ratio regarding the binding to the VAChT of the (−)-enantiomer in comparison to the racemic (+)-enantiomer. The comparison of this tracer to the reference tracer (−)-[^{18}F]FEOBV in the rat model showed that both tracers had rather similar properties but that a significantly better signal-to-noise ratio was demonstrated for (−)-[^{18}F]FBVM **11**, although a potential partial off-target binding cannot be excluded. Several characteristics of (−)-[^{18}F]FBVM **11** could explain why a higher *in vivo* contrast was obtained for it than for (−)-[^{18}F]FEOBV, such as the 50-fold better affinity measured in the same experimental conditions, and a lower binding to plasma proteins and peripheral defluorination. In view of these properties, (−)-[^{18}F]FBVM **11** could be more sensitive to detect *in vivo* the cholinergic denervation that occurs particularly in AD in brain areas having a lower density

of VAChT than the striatum, such as the cortex and hippocampus. The present study has several limitations and it will be necessary to explore more precisely the *in vivo* properties of (−)-[^{18}F]FBVM **11**, in particular in experimental pathological models of cholinergic denervation in rodents, and in physiological and pathological conditions in non-human primates. However, this new tracer is highly promising for future clinical applications.

4. Experimental section

4.1. Chemistry

^{1}H NMR and ^{13}C NMR spectra were recorded on a Bruker DPX 250 or 400 Mhz instrument using $CDCl_3$ and DMSO-d_6. The chemical shifts are reported in parts per million (δ scale), and all coupling constant (J) values are reported in hertz. The following abbreviations were used for the multiplicities: s (singlet), d (doublet), t (triplet), q (quartet), p (pentuplet), m (multiplet), sext (sextuplet), and dd (doublet of doublets). Melting points are uncorrected. IR absorption spectra were obtained on a PerkinElmer PARAGON 1000 PC, and the values are reported in inverse centimeters. HRMS spectra were acquired in positive mode with an ESI source on a Q-TOF mass by the "Fédération de Recherche" ICOA/CBM (FR2708) platform. Monitoring of the reactions was performed using silica gel TLC plates (silica Merck 60 F 254). Spots were visualized by UV light (254 nm and 356 nm). Column chromatography was performed using silica gel 60 (0.063–0.200 mm, Merck.). All reagents were purchased from commercial suppliers and were used without further purification.

4.1.1. 5-Fluoro-3-(4-phenylpiperidin-1-yl)-1,2,3,4-tetrahydronaphthalen-2-ol **3**

To an oven-dried tube reactor equipped with stirrer bar and a Teflon screw cap was added compound **2** [34] (849 mg, 2.6 mmol), $BF_3.Et_2O$ (818 µl, 6.6 mmol, 2.5 eq.) and 1,2-dichlorobenzene (9 ml). The mixture was cooled to 0 °C then *tert*BuONO (629 µl, 4.7 mmol, 1.8 eq.) was dropwise added *via* a syringe under argon atmosphere and 0 °C. The mixture was stirred at 0 °C for 15 min then a solution of PIDA (170 mg, 0.5 mmol, 0.2 eq.) in 1,2-dichlorobenzene (2 mL) was added. The reactor was sealed and heated to 40 °C for 36h. After cooling the mixture to r.t., solvent was removed under vacuum. The crude was solubilised in DCM (30 mL) and washed with a saturated aqueous solution of $NaHCO_3$ (30 mL), dried over $MgSO_4$, filtered. After removing the solvent under reduced pressure, the resulting crude was purified by flash chromatography using EP/EtOAc (10/0 to 1/1) as eluent to afford the desired **3** (500 mg, 59%) as a pale beige solid. Mp: 147–148 °C. IR (ATR diamond, v, cm^{-1}): 3434, 3079, 2931, 2910, 1579, 1492, 1462, 1411, 1376, 1278, 1141, 1003, 769, 711, 696. HRMS (ESI$^+$): calc. for $C_{21}H_{25}FNO$ $[M+H]^+$: 326. 19146 found: 326.19131.

^{1}H NMR (250 MHz, $CDCl_3$) δ 7.37–7.17 (m, 5H, 5H–Ar), 7.11 (td, J = 7.9, 5.7 Hz, 1H, H–Ar), 6.95–6.80 (m, 2H, 2 H–Ar), 4.34 (brs, 1H, OH), 3.87 (td, J = 10.2, 5.6 Hz, 1H, CH), 3.33 (dd, J = 16.2, 5.7 Hz, 1H, CH_2), 3.15–3.02 (m, 1H, CH_2), 3.02–2.84 (m, 3H), 2.83–2.50 (m, 4H), 2.44 (td, J = 11.5, 2.5 Hz, 1H, CH_2), 2.01–1.86 (m, 3H), 1.85–1.62 (m, 1H). ^{13}C NMR (63 MHz, $CDCl_3$) δ 161.1 (d, ^{1}J = 243.9 Hz, Cq), 146.2(Cq), 136.8 (d, ^{3}J = 4.3 Hz, Cq), 128.6 (2CH), 127.4 (d, ^{3}J = 8.7 Hz, CH), 127.0(2CH), 126.4 (CH), 124.7 (d, ^{4}J = 3.3 Hz, CH), 122.7 (d, ^{2}J = 17.6 Hz, Cq), 112.4 (d, ^{2}J = 21.9 Hz, CH), 66.2 (CH), 65.4(CH), 53.8(CH_2), 45.1 (CH_2), 43.0 (CH), 37.9 (d, ^{4}J = 2.2 Hz, CH_2), 34.5 (CH_2), 34.0 (CH_2), 19.2 (d, ^{4}J = 3.3 Hz, CH_2). ^{19}F NMR (235 MHz, $CDCl_3$) δ −117.3 (dd, J = 9.9, 5.5 Hz). HPLC PhenylHexyl-Phenomenex, 10 × 250 mm, ACN/ammonium acetate 0.1 M 70/30, 4 mL min^{-1} flow, retention time 11 min. HPLC Chiralpak IA, Daicel, 10 × 250 mm, eluent ACN/ammonium acetate 0.1 M 85/15, 4 mL min^{-1} flow, retention time Enantiomer 1: 18 min, retention time Enantiomer 2: 22 min, ratio 50/50.

4.1.2. General procedure for synthesis of Mosher's esters

In an oven-dried round-bottom flask, compound **3** (650 mg, 2.0 mmol) was solubilised in DCM (5 mL). DCC (515 mg, 2.5 mmol, 1.25 eq.), DMAP (5 mg, 0.4 mmol, 0.2 eq.) and (+)-(R)-Mosher acid (561 mg, 2.4 mmol, 1.2 eq.) were added respectively under argon atmosphere. The reaction mixture was left under stirring at r.t for 24h. The reaction was stopped by adding a saturated aqueous solution of $NaHCO_3$ (30 mL) and then transferred to a separating funnel. The organic layer was collected and the aqueous layer was extracted with DCM (2 x 30 mL). Then organic layers were combined together, dried over $MgSO_4$ and filtered. Solvent was removed under reduced pressure. The resulting crude was purified by flash chromatography on silica gel column using EP/EtOAc (100/0 to 95:5) as eluent to afford the desired products **4** (276 mg, 26%) and **5** (369 mg, 34%) as white amorphous solids.

4.1.3. (R)-(2R,3R)-5-fluoro-3-(4-phenylpiperidin-1-yl)-1,2,3,4-tetrahydronaphthalen-2-yl 3,3,3-trifluoro-2-methoxy-2-phenylpropanoate ***4***

HRMS (ESI$^+$): calc. for $C_{31}H_{32}F_4NO_3$ $[M+H]^+$: 542.23128 found: 542.23097. IR (ATR Diamond, *v*, cm^{-1}): 3060.5, 3002.6, 2947.0, 1738.2, 1588.1, 1496.7, 1384.4, 1187.1, 1079.8, 1054.2793.5, 763.0, 745.8, 736.7. ^{1}H NMR (250 MHz, $CDCl_3$) δ 7.80 (dd, *J* = 6.5, 3.1 Hz, 2H, 2H–Ar), 7.54–7.44 (m, 3H, 3 H–Ar), 7.41–7.31 (m, 2H, 2H–Ar), 7.31–7.21 (m, 3H, 3 H–Ar), 7.21–7.09 (m, 1H, 1 H–Ar), 7.02–6.80 (m, 2H, 2 H–Ar), 5.63 (td, *J* = 9.5, 5.9 Hz, 1H, CH), 3.78 (s, 3H, OMe), 3.32–3.09 (m, 4H), 3.07–2.76 (m, 4H), 2.64–2.40 (m, 2H), 2.02–1.62 (m, 4H). ^{13}C NMR (63 MHz, $CDCl_3$) δ 166.0 (Cq), 160.7 (d, ^1J = 244.5 Hz, Cq), 146.5 (Cq), 135.7 (d, ^4J = 4.4 Hz, Cq), 132.6 (Cq), 129.8 (CH), 128.6 (4CH), 127.8 (2CH), 127.5 (d, ^3J = 8.6 Hz, CH), 126.9 (2CH), 126.3 (CH), 124.0 (d, ^3J = 3.3 Hz, CH), 123.5 (q, ^1J = 288.9, CF_3),122.5 (d, ^2J = 17.7 Hz, Cq), 112.9 (d, ^2J = 21.8 Hz, CH), 85.0 (q, ^2J = 27.4 Hz, Cq), 71.2 (CH), 63.2 (CH), 55.70 (d, ^4J = 1.5 Hz, CH_3), 52.8 (CH_2), 46.8 (CH_2), 42.9 (CH), 34.8 (d, ^4J = 2.1 Hz, CH_2), 34.5 (CH_2), 33.2 (CH_2), 19.9 (d, ^4J = 2.9 Hz, CH_2). ^{19}F NMR (235 MHz, $CDCl_3$) δ −71.1, −117.8 (dd, *J* = 9.4, 5.7 Hz).

4.1.4. (R)-(2S,3S)-5-fluoro-3-(4-phenylpiperidin-1-yl)-1,2,3,4-tetrahydronaphthalen-2-yl 3,3,3-trifluoro-2-*methoxy-2-phenylpropanoate* ***5***

HRMS (ESI$^+$): calc. for $C_{31}H_{32}F_4NO_3$ $[M+H]^+$: 542.23128 found: 542.23125. IR (ATR Diamond, *v*, cm^{-1}): 3025.6, 2978.2, 2497.9, 1746.9, 1619.3, 1584.5, 1493.1, 1397.5, 1293.4, 1166.1, 1012.2, 966.5, 786.5, 699.7. ^{1}H NMR (250 MHz, $CDCl_3$) δ 7.74–7.61 (m, 2H, 2H–Ar), 7.47–7.38 (m, 3H, 3H–Ar), 7.34–7.26 (m, 2H, 2H–Ar), 7.23–7.06 (m, 4H, H–Ar), 6.94–6.83 (m, 2H,H–Ar), 5.51 (td, *J* = 8.6, 5.5 Hz, 1H, CH), 3.63 (q, *J* = 1.2 Hz, 3H, OMe), 3.34 (dd, *J* = 16.2, 5.6 Hz, 1H, CH_2), 3.15–2.73 (m, 6H), 2.51 (td, *J* = 11.3, 2.7 Hz, 1H, CH_2), 2.42–2.22 (m, 2H), 1.67 (dtq, *J* = 28.9, 12.2, 4.0 Hz, 4H, $2CH_2$). ^{13}C NMR (63 MHz, $CDCl_3$) δ 166.0 (Cq), 160.7 (d, ^1J = 244.8 Hz, Cq), 146.5 (Cq), 135.6 (d, ^4J = 4.4 Hz, Cq), 132.4 (Cq), 129.7 (CH), 128.5 (2CH), 128.5 (2CH), 127.8 (2CH), 127.5 (d, ^3J = 8.6 Hz, CH), 126.9 (2CH), 126.2 (CH), 124.0 (d, ^4J = 3.4 Hz, CH),123.5 (q, ^1J = 288.6 Hz, CF_3), 122.7 (d, ^2J = 17.7 Hz, Cq), 113.0 (d, ^2J = 21.7 Hz, CH), 84.7 (q, ^2J = 27.5 Hz, Cq), 72.3 (CH), 62.6 (CH_2), 55.7 (CH_3), 51.3 (CH_2), 48.7 (CH_2), 42.8 (CH), 34.7 (d, ^4J = 2.2 Hz, CH_2), 34.2 (CH), 33.6 (CH_2), 21.3 (d, ^4J = 3.1 Hz, CH_2). ^{19}F NMR (235 MHz, $CDCl_3$) δ −71.84, −118.06 (dd, *J* = 9.5, 5.7 Hz).

4.1.5. 1-((2R,3R)-8-fluoro-3-(((R)-3,3,3-trifluoro-2-methoxy-2-phenylpropanoyl)oxy)-1,2,3,4-tetrahydronaphthalen-2-yl)-4-phenylpiperidin-1-ium chloride ***4•HCl***

In a round bottom flask, **4** (250 mg, 0.46 mmol) was solubilised in dry dioxane (3 mL) and the solution cooled to 0 °C. A 4 N HCl solution in dioxane (173 µL, 0.69 mmol, 1.5 eq.) was added dropwise and was left under stirring at r.t for 24h. Solvent and excess of HCl were removed slowly under atmospheric pressure to afford crystals. The crude was then triturated with Et_2O to obtain needles, which were collected by filtration and then dried under vacuum to obtain **4•HCl** in quantitative yield. Crystals were collected for XRD analysis. Mp: 168–169 °C. IR (*v* cm^{-1}): 3028.3, 1748.3, 1590.4, 1470.3, 1245.0, 1163.4, 963.9, 845.0, 700.1, 664.1, 552.4. ^{1}H NMR (250 MHz, DMSO-d_6) δ 11.62 (bs, 1H, NH), 7.48 (s, 5H, H–Ar), 7.40–7.30 (m, 2H, H–Ar), 7.29–7.12 (m, 4H, H–Ar), 7.10–6.92 (m, 2H, H–Ar), 5.95 (d, *J* = 4.9 Hz, 1H, CH), 3.99–3.83 (m, 1H, CH), 3.79–2.90 (m, 11H), 2.88–2.67 (m, 1H, CH), 2.27 (d, *J* = 14.0 Hz, 2H, CH_2), 2.07–1.86 (m, 2H, CH_2). ^{13}C NMR (63 MHz, DMSO-d_6) δ 164.7 (Cq), 159.1 (d, ^1J = 244.2 Hz, Cq), 144.1 (Cq), 135.5 (d, ^4J = 2.9 Hz, Cq), 130.7 (Cq), 130.0 (CH), 128.8 (2CH), 128.6 (2CH), 128.2 (d, ^3J = 8.2 Hz, CH), 127.2 (2CH), 126.6 (3CH), 124.2 (CH),123.1 (q, ^1J = 290.4 Hz, CF_3) 119.7 (d, ^2J = 16.5 Hz, Cq), 113.4 (d, ^2J = 20.9 Hz, CH), 84.2 (q, ^2J = 27.2, 26.6 Hz, Cq), 71.9 (CH), 63.14 (CH), 55.6 (CH_3), 50,6 (CH_2), 49.3 (CH_2), 39.2 (CH), 32.6 CH_2, 29.8 (CH_2), 29.6 (CH_2), 20.7 (CH_2). ^{19}F NMR (235 MHz, DMSO-d_6) δ −70.9, −119.9 (dd, *J* = 9.1, 5.8 Hz).

4.1.6. (2R,3R)-5-fluoro-3-(4-phenylpiperidin-1-yl)-1,2,3,4-tetrahydronaphthalen-2-ol ((−)-(R,R)-5-FBVM) ***6***

In a round-bottom flask compound **4** (96 mg, 0.14 mmol) was solubilised in 1,4-dioxane (3 mL) then 1 M aqueous solution of NaOH (3 mL) was added and the reaction mixture was left under stirring at 50 °C for 18h. Solvents were removed under reduced pressure then the resulting crude was solubilised in water and extracted with EtOAc (3 x 5 mL). Organic layers were combined together and dried over $MgSO_4$. Solvent was removed under reduced pressure to afford the desired product **6** as a pale beige solid (48 mg, 83%). $\mathbf{[\alpha_D]^{20}}$ = −82.0 (*c* = 0.01 g/mL Chloroform). Mp: 148–149 °C. IR (ATR Diamond, *v*, cm^{-1}): 3379, 3062, 3027, 2937, 2771, 1618, 1601, 1578, 1413, 1325, 1238, 1161, 1022, 1003, 977, 804, 758. HRMS (ESI$^+$): calc. for $C_{21}H_{25}FNO$ $[M+H]^+$: 326. 19146 found: 326.1913. ^{1}H NMR (250 MHz, $CDCl_3$) δ 7.37–7.17 (m, 5H, H–Ar), 7.11 (td, *J* = 7.9, 5.7 Hz, 1H, H–Ar), 6.95–6.80 (m, 2H, H–Ar), 4.34 (brs, 1H, OH), 3.87 (td, *J* = 10.2, 5.6 Hz, 1H, CH), 3.33 (dd, *J* = 16.2, 5.7 Hz, 1H, CH_2), 3.15–3.02 (m, 1H, CH_2), 3.02–2.84 (m, 3H), 2.83–2.50 (m, 4H), 2.44 (td, *J* = 11.5, 2.5 Hz, 1H, CH_2), 2.01–1.86 (m, 3H), 1.85–1.62 (m, 1H). ^{13}C NMR (63 MHz, $CDCl_3$) δ 161.1 (d, ^1J = 243.9 Hz, Cq), 146.2(Cq), 136.8 (d, ^4J = 4.3 Hz, Cq), 128.6 (2CH), 127.4 (d, ^3J = 8.7 Hz, CH), 127.0 (2CH), 126.4 (CH), 124.7 (d, ^4J = 3.3 Hz, CH), 122.7 (d, ^2J = 17.6 Hz, Cq), 112.4 (d, ^2J = 21.9 Hz, CH), 66.2 (CH), 65.4 (CH), 53.8 (CH_2), 45.1 (CH_2), 43.0 (CH), 37.9 (d, ^4J = 2.2 Hz, CH_2), 34.5 (CH_2), 34.0 (CH_2), 19.2 (d, ^4J = 3.3 Hz, CH_2). ^{19}F NMR (235 MHz, $CDCl_3$) δ −117.3 (dd, *J* = 9.9, 5.5 Hz). HPLC

Chriralpak IA, Daicel, 10 × 250 mm, eluent ACN/ammonium acetate 0.1 M 85/15, 4 mL min^{-1} flow, retention time 18 min.

4.1.7. (2S,3S)-5-fluoro-3-(4-phenylpiperidin-1-yl)-1,2,3,4-tetrahydronaphthalen-2-ol ((+)- (S,S)- 5-FBVM) ***7***

In a round-bottom flask compound **5** (100 mg, 0.17 mmol) was solubilised in 1,4-dioxane (3 mL) then 1 M aqueous solution of NaOH (3 mL) was added and the reaction mixture was left under stirring at 50 °C for 18h. Solvents removed under reduced pressure then the resulting crude was solubilised in water and extracted with EtOAc (3 x 5 mL). Organic layers were combined together and dried over $MgSO_4$. Solvent was removed under reduced pressure to afford the desired product **7** as pale beige solid (56 mg, 99%). $\mathbf{[\alpha_D]^{20}}$ = +82.8 (*c* = 0.01 g/mL Chloroform). Mp:148–149 °C. IR (*v* cm^{-1}): 3379, 3064, 2771, 1619, 1578, 1492, 1374, 1218, 1161, 1073, 791. HRMS (ESI^+): calc. for $C_{21}H_{25}FNO$ $[M+H]^+$: 326.19146 found: 326.1913. ^{1}H NMR (250 MHz, $CDCl_3$) δ 7.37–7.17 (m, 5H, H–Ar), 7.11 (td, *J* = 7.9, 5.7 Hz, 1H, H–Ar), 6.95–6.80 (m, 2H, H–Ar), 4.34 (brs, 1H, OH), 3.87 (td, *J* = 10.2, 5.6 Hz, 1H, CH), 3.33 (dd, *J* = 16.2, 5.7 Hz, 1H, CH_2), 3.15–3.02 (m, 1H, CH_2), 3.02–2.84 (m, 3H), 2.83–2.50 (m, 4H), 2.44 (td, *J* = 11.5, 2.5 Hz, 1H, CH_2), 2.01–1.86 (m, 3H), 1.85–1.62 (m, 1H, H of CH_2). ^{13}C NMR (63 MHz, $CDCl_3$) δ 161.1 (d, ^1J = 243.9 Hz, Cq), 146.2(Cq), 136.8 (d, ^4J = 4.3 Hz, Cq), 128.6 (2CH), 127.4 (d, ^3J = 8.7 Hz, CH), 127.0 (2CH), 126.4 (CH), 124.7 (d, ^4J = 3.3 Hz, CH), 122.7 (d, ^2J = 17.6 Hz, Cq), 112.4 (d, ^2J = 21.9 Hz, CH), 66.2 (CH), 65.4 (CH), 53.8 (CH_2), 45.1(CH_2), 43.0 (CH), 37.9 (d, ^4J = 2.2 Hz, CH_2), 34.5 (CH_2), 34.0 (CH_2), 19.2 (d, ^4J = 3.3 Hz, CH_2). ^{19}F NMR (235 MHz, $CDCl_3$) δ −117.3 (dd, *J* = 9.9, 5.5 Hz). HPLC Chiralpak IA, Daicel, 10 × 250 mm, eluent ACN/ammonium acetate 0.1 M 85/15, 4 mL min^{-1} flow, retention time 22 min.

*4.1.8. 5-Iodo-3-(4-phenylpiperidin-1-yl)-1,2,3,4-tetrahydronaphthalen-2-ol (****5-IBVM****)* ***8***

In a round bottom flask, compound **2** (1.00 g, 3.10 mmol) was solubilised in CH_3CN (18 mL) then PTSA.H_2O (1.80 g, 9.32 mmol, 3.0 eq.) was added in one portion. The mixture was cooled down to 0 °C then a solution of $NaNO_2$ (428 mg, 6.2 mmol, 2.0 eq.) and KI (1.20 g, 7.75 mmol, 2.5 eq.) in water (5 mL) was added. After stirring at 0 °C for 15 min, the reaction mixture was allowed to warm up to r.t and left under stirring for 4h. Water (17 mL) and a $NaHCO_3$ saturated solution (35 mL) were added. The aqueous layer was extracted with EtOAc (3 x 25 mL) and the combined organic layers were dried over $MgSO_4$, filtered then dried under reduced pressure. The residue was purified by flash chromatography on silica gel column (PE/EtOAc: 85/15) to afford the desired **8** as a yellowish solid (587 mg, 50%). ^{1}H NMR (250 MHz, $CDCl_3$) δ 7.70 (d, *J* = 7.8 Hz, 1H, H–Ar), 7.39–7.16 (m, 6H, H–Ar), 7.10 (d, *J* = 7.7 Hz, 1H, H–Ar), 6.83 (t, *J* = 7.7 Hz, 1H, OH), 3.83 (td, *J* = 10.2, 5.6 Hz, 1H, CH), 3.24–2.33 (m, 12H).

4.1.9. 3-(4-Phenylpiperidin-1-yl)-5-(4,4,5,5-tetramethyl-1,3,2-dioxaborolan-2-yl)-1,2,3,4-tetrahydronaphthalen-2-ol ***9***

In an oven-dried tube, **8** (100 mg, 0.23 mmol) was solubilised in degassed anhydrous DMF (2 mL) then B_2Pin_2 (88 mg, 0.35 mmol, 1.5 eq.), KOAc (68 mg, 0.69 mmol, 3.0 eq.) and Pd(dppf)Cl_2.DCM (19 mg, 0.02 mmol, 0.1 eq.) were added successively. The tube was sealed under argon and heated up to 160 °C for 1h30. The reaction mixture was cooled to r.t then DMF was removed under reduced pressure. The residue was washed with brine (20 mL) and filtered on a pad of celite. The filtrate was extracted by EtOAc (3 x 10 mL). Organic layers were combined, dried over $MgSO_4$ and filtered. After removing solvent under reduced pressure, the residue was purified by flash chromatography on silica gel column (PE/EtOAc 85/15 and 5% of Et_3N) to afford the desired product **9** as a white solid (50 mg, 44%) which was readily used to prevent degradation. R_f: 0.27 (PE/EtOAc 85/15). ^{1}H NMR (400 MHz, $CDCl_3$) δ 7.62 (dd, *J* = 7.1, 1.7 Hz, 1H, HAr), 7.37–7.24 (m, 4H, 4H–Ar), 7.24–7.09 (m, 3H, 3xHAr), 3.87 (td, *J* = 10.2, 5.8 Hz, 1H, CH), 3.45 (dd, *J* = 16.7, 4.7 Hz, 1H, H of CH_2), 3.29 (dd, *J* = 15.9, 5.8 Hz, 1H, H of CH_2), 3.04–2.71 (m, 6H, CH and CH_2 and 3H of CH_2), 2.57 (tt, *J* = 11.9, 3.9 Hz, 1H, CH), 2.39 (td, *J* = 11.5, 2.3 Hz, 1H, H of CH_2), 1.97–1.83 (m, 3H, H of CH_2 and CH_2), 1.76 (m, 1H, H of CH_2), 1.37 (s, 12H, 4xCH_3). ^{13}C NMR (101 MHz, $CDCl_3$) δ 146.4 (Cq), 141.4 (Cq), 134.0 (CH), 133.8 (Cq), 132.4 (CH), 128.6 (2CH and Cq), 127.0 (2CH), 126.3 (CH), 125.5 (CH), 83.7 (2Cq), 67.0 (CH), 65.6 (CH), 53.9 (CH_2), 45.4 (CH_2), 43.1 (CH), 38.6 (CH_2), 34.6 (CH_2), 34.1 (CH_2), 26.3 (CH_2), 25.2 (2CH_3), 25.0 (2CH_3). IR (*v* cm^{-1}): 3424, 3030, 2972, 2942, 2916, 2855, 2805, 1587, 1493, 1470, 1450, 1428, 1385, 1371, 1349, 1316, 1265, 1141, 1127, 1112, 1066, 1052, 1003, 986, 967, 858, 827, 794.4, 774, 756, 726, 699, 666, 635. HRMS (ESI^+): calc. for $C_{27}H_{37}BNO_3$ $[M+H]^+$: 434.2861, found: 434.2866.

4.2. Crystallography

Crystallographic data of compound **4** were collected at 150 K with an Bruker APEX-II diffractometer using monochromatic Mo-Ka radiation (0.71073 Å). The collected data were reduced using the Saint software suite (Bruker

AXS Inc., Madison, Wisconsin, USA). Then absorption correction was performed using the SADABS software (*SADABS.* Bruker AXS Inc., Madison, Wisconsin, USA). The crystal structure was solved by direct methods using ShelxT and refined against F^2 by full least square method within the OLEX2 program [67,68] also used for drawings. Full crystallographic results have been deposited at the Cambridge Crystallographic Data Centre (CCDC 2104956, www.ccdc.cam.ac.uk/structures).

4.3. Radiochemistry

4.3.1. General

No-carrier-added aqueous ^{18}F-fluoride ion was produced on a cyclotron (PET trace, GE Healthcare) by irradiation of enriched ^{18}O H_2O with protons via the $^{18}O(p,n)^{18}F$ nuclear reaction. ^{18}F Fluoride was transferred to a modified TRACERlab FX-FN Pro (GE) synthesizer and passed through an anion-exchange resin (Waters Sep-Pak Accell Light QMA cartridge in the carbonate form).

4.3.2. Synthesis of (rac)-[^{18}F]-FBVM 10

Trapped ^{18}F-fluoride was isolated by elution with 550 µL of aqueous solution of eluent solution containing KOTf (5 mg) and K_2CO_3 (50 µg). Azeotropic drying by addition of ACN (1 mL) was performed. The evaporation was performed at 90 °C under helium flow and vacuum, and the operation was repeated twice prior to nucleophilic substitution. Precursor **8** (2 mg) with $Cu(OTf)_2$ (3.6 mg) dissolved in DMF (960 µL) and pyridine (40 µL) were added to the reactive fluorine ions. The reaction was heated at 100 °C for 10 min, then cooled to 30 °C and diluted with water (8 mL). The crude medium was passed through a *t*C18 plus cartridge (Waters) and rinsed with additional water (4 mL) to trap the desired compound and remove most polar derivatives. Crude **(*rac*)-[^{18}F]-FBVM** 10 was eluted from the cartridge by CAN (2 mL) and diluted with ammonium acetate 0.1 M (1 mL). The solution was loaded onto the HPLC loop of the synthesizer and purified on a semi-preparative column (Luna PhenylHexyl-Phenomenex, 10 × 250 mm) using ACN/ammonium acetate 0.1 M 70/30 as mobile phase at a 4 mL min^{-1} flow. Under this condition the **(*rac*)-[^{18}F]-FBVM** was collected around 11 min. The collected fraction was diluted with water (30 mL) and trapped on a *t*C18 light cartridge. **(*rac*)-[^{18}F]-FBVM** was eluted from the cartridge by 0.8 mL f injectable ethanol and formulation was completed by the addition of 7.2 mL of saline.

4.3.3. Synthesis of (−)-(R,R)-5-[^{18}F]FVBM 11 and (+)-(S,S)-5-[^{18}F]FBVM 12

The production of isolated enantiopure probes occurred following the radiosynthesis of **(+/−)-5-[^{18}F]FBVM 10** completed by a chiral HPLC purification. The collected HPLC fraction of pure **(+/−)-5-[^{18}F]FBVM 10** was loaded onto the loop of the synthesizer and purified on a semi-preparative chiral column (Chiralpak IA, Daicel, 10 × 250 mm) using ACN/ammonium acetate 0.1 M 85/15 as mobile phase at a 4 mL min^{-1} flow. Under these conditions the **(−)-[^{18}F]FVBM 11** was selectively collected around 18 min and **(+)[^{18}F]FBVM 12** around 22 min. The enantiomerically pure fractions (−) or (+) were diluted with water (35 mL) and trapped on a *t*C18 light cartridge. **(−)-([^{18}F]FVBM 11** and **(+)-[^{18}F]FBVM 12** was eluted from the cartridge by 0.8 mL of injectable ethanol and formulation was completed by the addition of 7.2 mL of saline. As we identified that the most active compound was **(−)[^{18}F]FVBM 11** and thus the first eluted peak from the chiral purification, we modified the production to obtain it in a single HPLC purification. Alternatively, the use of ACN/ammonium acetate 0.1 M/MeOH:70/10/20 as mobile phase at a 4 mL min^{-1} flow led to **(−) [^{18}F]FVBM 11** with a retention time of 14 min. The formulation was achieved as previously reported. Using this method we were able to achieve **(−)[^{18}F]FVBM 11** production and formulation in 68 ± 3 min.

4.3.4. Quality control

Radiotracers were controlled by analytical HPLC equipped with UV and radio detectors. The **(*rac*)-[^{18}F]- FBVM 10** purity was checked using an analytical column (Phenomenex Luna 5µ Phenyl Hexyl 4,6 × 250 mm) using ACN/Ac Am 0,1 M 70/30 as mobile phase at a 1 mL/min flow. Under these conditions, the time retention was 9 min. In the case of enantiomeric purification, additionally to the previous control, a HPLC control using a chiral column (Chiralpak IA 4,6 × 250 mm 5 µ) was used to evaluate the enantiomeric purity of either **(−) [^{18}F]FVBM 11** or **(+) [^{18}F]FBVM 12**. For this control, ACN/Ac Am 0.1 M 85/15 was used as mobile phase at a 1 mL/min flow. Under these conditions the time retention of **(−) [^{18}F]FVBM 11** and **(+) [^{18}F]FBVM 12** were respectively 16.2 and 21.1 min. For all compounds,

radiochemical purity was better than 99%, molar activity higher than 100 GBq/µmole and no degradation was observed in the formulation media nor in serum for at least 4h.

4.3.5. Synthesis of (−)-[^{18}F]FEOBV

The tracer was prepared using an method adapted from the original process described by Mulholland et al. [21]. The corresponding enantiomerically pure precursor ((−)-TEBV, 1.5 mg) was used for the one step radiolabeling of (−)-[^{18}F]FEOBV. The [^{18}F]fluoride was eluted from the cartridge using an aqueous eluent solution (3 mg of K_2CO_3 diluted in 230 µL of pure water and 5.8 mg of Kryptofix$_{222}$ diluted in 570 µL of acetonitrile). Azeotropic drying by addition of ACN (1 mL) was performed. The evaporation was performed at 90 °C under helium flow and vacuum, and the operation was repeated twice. The precursor (1.5 mg) dissolved in ACN (0.7 mL) was transferred to the reactor and heated at 115 °C for 7.5 min. The medium was cooled to 40 °C, diluted with water (8 mL) and passed through a *t*-C18 cartridge. Then, the cartridge was rinsed with water (5 mL), eluted with ACN (2 mL) and diluted with water (1 mL). The crude solution was injected to the loop and purified by HPLC using ACN/ammonium acetate 0.1 M (60/40) at a 4 mL/min flow. The (−)-[^{18}F]FEOBV was collected with a time retention of 15 min, diluted with water (40 mL) and the solution was passed through a light t-C18 cartridge. The cartridge was rinsed with water (5 mL), eluted with 500 µL of ethanol and the formulation was completed by the addition of 3.5 mL of 0.9% NaCl. The radiosynthesis was achieved in 80 ± 3 min with a RCY of 71 ± 10.1% and a molar activity of 248.9 ± 56.4 GBq/µole.

4.3.6. Stability

The stability in plasma of the injectable solution (**(*rac*)-[^{18}F]-FBVM 10**) was checked by HPLC up to 4 h after the end of preparation. To conduct this control,100 µl of the radiotracer solution was mixed with 1 ml of rat plasma and incubated at 37C. Then, 500 µl of acetonitrile were added, the organic layer was removed and filtered, 20 µl was loaded onto the HPLC, and the stability was checked at a 4-h time point after production. The radiochemical stability was also checked up to 4h after the end of preparation. The HPLC conditions used to check the chemical and plasmatic stability are those reported above in quality control using the Luna column. No degradation was observed.

4.4. Biological studies

4.4.1. Animals

Experiments were performed on male Wistar rats weighing 280–320 g (Centre d'Elevage R. Janvier, Le Genest St Isle, France). All animal procedures were conducted in accordance with the requirements of the European Community Council Directive 2010/63/EU for the care of laboratory animals and with the authorization of the Regional Ethical Committee (N° APAFIS#4208–2016022218004689 v3 and APAFIS#26811–2020073110598684 v2).

4.4.2. In vitro binding studies

The Ki towards VAChT was measured for stable (+/−)-FBVM **3**, (+)-FBVM **7**, (−)-FBVM **6**, (+/−)FEOBV and (−)FEOBV on a membrane preparation from rat brain hemispheres according to a modified version of a previously described method (Scheunemann et al., 2004). Stable L-(−)-vesamicol was obtained from Sigma Aldrich (Saint-Quentin-Fallavier, France) and [^{3}H]vesamicol (molar activity 1705.7 GBq/mmol) from Perkin-Elmer (Courtaboeuf, France). The IC_{50} values were determined graphically for each compound and the Ki was calculated according to Cheng and Prussof [48]. The results were expressed as mean Ki ± SEM from 3 independent experiments.

4.4.3. Biodistribution studies

Each tracer, (+/−)-[^{18}F]FBVM **10**, (+)-[^{18}F]FBVM **12**, (−)-[^{18}F]FBVM **11** and (−)-[^{18}F]FEOBV was evaluated in two groups of rats (one control group and one VES group, n = 5–9/group). Animals were injected i.v. under isoflurane gas anesthesia (Baxter, France; 4% in O2) in the penis vein with 3.61–8.18 MBq of one of these tracers dissolved in 0.3 mL of saline. In the VES groups, injection of the tracer was preceded (5 min) by i.v. injection of vesamicol (L-(−)-vesamicol, Sigma Aldrich, Saint-Quentin-Fallavier, France) at the dose of 0.5 µmol/kg.

In a 2nd set of experiments, (−)-[^{18}F]FBVM **11** and (−)-[^{18}F]FEOBV were evaluated in two other groups of rats (one control group and one HAL group, n = 6/group). In the HAL group, injection of the tracer was preceded (5 min) by i.v. injection of haloperidol (Haldol®, Janssen, 2 mg/ml) at the dose of 1 mg/kg (2.6 µmol/kg).

All animals were killed by decapitation at 2 h post injection of the tracer. The whole brain was quickly removed and dissected into cortex, striatum, hippocampus, thalamus and cerebellum. A fraction of blood and bone were also removed. Samples were weighed and radioactivity was measured in a γ counter (2480 Gamma counter Wizard, Perkin Elmer), and the percentage of injected dose per gram of tissue (%ID/g) was calculated by comparison with samples to standard dilutions of the injected solution.

4.4.4. PET acquisition and data analysis

The rats received an i.v. injection of around 37 MBq of (+/−)-[^{18}F]FBVM **10**, (+)-[^{18}F]FBVM **12**, (−)-[^{18}F]FBVM **11** or (−)-[^{18}F]FEOBV (n = 2–4 rats/tracer). Acquisitions were made on a microPET-CT SuperArgus system (Sedecal, Madrid, Spain), which has an effective axial/trans axial field of view (FOV) of 4.8/6.7 cm, a spatial resolution less than 2 mm and a sensitivity above 2.5% in the whole FOV. Animals were anesthetized with isoflurane, at 3% in O2 for induction and then 1.5–2% during scanning. Each acquisition lasted 121 min and PET list-mode scans were rebinned into 1 frame of 1 min followed by 12 frames of 10 min. Each PET scan was corrected for random, scatter, and attenuation, and the images were reconstructed using a 2-D OSEM algorithm (GE Healthcare, France) into voxels of 0.3875 × 0.3875 × 0.775 mm^3.

Author contributions : JV: supervision of radiochemistry, radiochemistry experiments and analyses of radiotracers; FB: supervision of chemistry; SS: PET imaging experiments; NR, HM, RBO: chemical synthesis and analysis of compounds; AC, NP, FS: structural analysis; ZG: *in vitro* experiments; GC, AD: radiochemistry experiments and analyses of radiotracers; SB, JB: animal experiments; DG: conceptualization; MM: crystallography data; PE: conceptualization; SR & SC: conceptualization, co-supervision, writing.

All authors contributed to the article and approved the submitted version.

Declaration of competing interest : The authors declare that they have no known competing financial interests or personal relationships that could have appeared to influence the work reported in this paper.

Acknowledgments : The authors thank the Région Centre Val de Loire (RTR MotivHealth, APR IR Imadach and Bialz); FEDER projects CHembio FEDER-FSE 2014-2020-EX003677 and Techsab FEDER-FSE 2014-2020-EX011313; SFR FED4226; Labex programs SYNORG (ANR-11-LABX-0029) and IRON (ANR-11-LABX-0018-01) for their financial support. They also thank Dr E. Rowley-Jolivet for English editing.

Appendix A. Supplementary data : The following is the Supplementary data to this article: Download : Download Word document (4MB)

Abbreviations :
AD - Alzheimer's disease
PD - Parkinson's disease
PDD - Parkinson's disease dementia
DLB - dementia with Lewy body
PET - Positron emission tomography
VAChT - vesicular acetylcholine transporter
FEOBV – fluoroethoxybenzovesamicol
FBVM - fluorobenzovesamicol

Data availability : No data was used for the research described in the article.

References

1. G. Deuschl, E. Beghi, F. Fazekas, T. Varga, K.A. Christoforidi, E. Sipido, C.L. Bassetti, T. Vos, V.L. Feigin. The burden of neurological diseases in Europe: an analysis for the global burden of disease study 2017. Lancet Public Health, 5 (10) (2020 Oct), pp. e551-e567, 10.1016/S2468-2667(20)30190-0
2. R.M. Ahmed, E.M. Devenney, M. Irish, A. Ittner, S. Naismith, L.M. Ittner, J.D. Rohrer, G.M. Halliday, A. Eisen, J.R. Hodges, M.C. Kiernan. Neuronal network disintegration: common pathways linking neurodegenerative diseases. J. Neurol. Neurosurg. Psychiatry, 87 (11) (2016 Nov), pp. 1234-1241, 10.1136/jnnp-2014-308350
3. H. Wilson, M. Politis, E.A. Rabiner, L.T. Middleton. Novel PET biomarkers to disentangle molecular pathways across age-related neurodegenerative diseases. Cells, 9 (12) (2020 Dec 2), p. 2581, 10.3390/cells9122581
4. P. Davies, A.J. Maloney. Selective loss of central cholinergic neurons in Alzheimer's disease. Lancet, 2 (8000) (1976 Dec 25), p. 1403, 10.1016/s0140-6736(76)91936-xISTEX
5. P.J. Whitehouse, R.G. Struble, J.C. Hedreen, A.W. Clark, C.L. White, I.M. Parhad, D.L. Price. Neuroanatomical evidence for a cholinergic deficit in Alzheimer's disease. Psychopharmacol. Bull., 19 (3) (1983), pp. 437-440
6. H. Hampel, M.M. Mesulam, A.C. Cuello, M.R. Farlow, E. Giacobini, G.T. Grossberg, A.S. Khachaturian, A. Vergallo, E. Cavedo, P.J. Snyder, Z.S. Khachaturian. The cholinergic system in the pathophysiology and treatment of Alzheimer's disease. Brain, 141 (7) (2018 Jul 1), pp. 1917-1933, 10.1093/brain/awy132
7. J.T. O'Brien, S.J. Colloby, S. Pakrasi, E.K. Perry, S.L. Pimlott, D.J. Wyper, I.G. McKeith, E.D. Williams. Alpha4beta2 nicotinic receptor status in Alzheimer's disease using 123I-5IA-85380 single-photon-emission computed tomography. J. Neurol. Neurosurg. Psychiatry, 78 (4) (2007 Apr), pp. 356-362, 10.1136/jnnp.2006.108209ISTEX
8. E.M. Mitsis, K.M. Reech, F. Bois, G.D. Tamagnan, M.G. Macavoy, J.P. Seibyl, J.K. Staley, C.H. van Dyck. 123I-5-IA-85380 SPECT imaging of nicotinic receptors in Alzheimer disease and mild cognitive impairment. J. Nucl. Med., 50 (9) (2009 Sep), pp. 1455-1463, 10.2967/jnumed.109.064030
9. K. Kendziorra, H. Wolf, P.M. Meyer, H. Barthel, S. Hesse, G.A. Becker, J. Luthardt, A. Schildan, M. Patt, D. Sorger, A. Seese, H.J. Gertz, O. Sabri. Decreased cerebral α4β2* nicotinic acetylcholine receptor availability in patients with mild cognitive impairment and Alzheimer's disease assessed with positron emission tomography. Eur. J. Nucl. Med. Mol. Imag., 38 (3) (2011 Mar), pp. 515-525, 10.1007/s00259-010-1644-5ISTEX
10. H. Okada, Y. Ouchi, M. Ogawa, M. Futatsubashi, Y. Saito, E. Yoshikawa, T. Terada, Y. Oboshi, H. Tsukada, T. Ueki, M. Watanabe, T. Yamashita. Magata Y.Alterations in α4β2 nicotinic receptors in cognitive decline in Alzheimer's aetiopathology. Brain, 136 (Pt 10) (2013 Oct), pp. 3004-3017, 10.1093/brain/awt195
11. M. Fujita, M. Ichise, S.S. Zoghbi, J.S. Liow, S. Ghose, D.C. Vines, J. Sangare, J.Q. Lu, V.L. Cropley, H. Iida, K.M. Kim, R.M. Cohen, W. Bara-Jimenez, B. Ravina, R.B. Innis. Widespread decrease of nicotinic acetylcholine receptors in Parkinson's disease. Ann. Neurol., 59 (1) (2006 Jan), pp. 174-177, 10.1002/ana.20688ISTEX
12. A. Kas, M. Bottlaender, J.D. Gallezot, M. Vidailhet, G. Villafane, M.C. Grégoire, C. Coulon, H. Valette, F. Dollé, M.J. Ribeiro, P. Hantraye, P. Remy. Decrease of nicotinic receptors in the nigrostriatal system in Parkinson's disease. J. Cerebr. Blood Flow Metabol., 29 (9) (2009 Sep), pp. 1601-1608, 10.1038/jcbfm.2009.74
13. P.M. Meyer, K. Strecker, K. Kendziorra, G. Becker, S. Hesse, D. Woelpl, A. Hensel, M. Patt, D. Sorger, F. Wegner, D. Lobsien, H. Barthel, P. Brust, H.J. Gertz, O. Sabri, J. Schwarz. Reduced alpha4beta2*-nicotinic acetylcholine receptor binding and its relationship to mild cognitive and depressive symptoms in Parkinson disease. Arch. Gen. Psychiatr., 66 (8) (2009 Aug), pp. 866-877, 10.1001/archgenpsychiatry.2009
14. D.E. Kuhl, R.A. Koeppe, S. Minoshima, S.E. Snyder, E.P. Ficaro, N.L. Foster, K.A. Frey, M.R. Kilbourn. In vivo mapping of cerebral acetylcholinesterase activity in aging and Alzheimer's disease. Neurology, 52 (4) (1999 Mar 10), pp. 691-699, 10.1212/wnl.52.4.691
15. H. Shinotoh, H. Namba, M. Yamaguchi, K. Fukushi, S. Nagatsuka, M. Iyo, M. Asahina, T. Hattori, S. Tanada, T. Irie. Positron emission tomographic measurement of acetylcholinesterase activity reveals differential loss of ascending cholinergic systems in Parkinson's disease and progressive supranuclear palsy. Ann. Neurol., 46 (1) (1999 Jul), pp. 62-69.
16. N.I. Bohnen, D.I. Kaufer, R. Hendrickson, L.S. Ivanco, B.J. Lopresti, G.M. Constantine, Mathis ChA, J.G. Davis, R.Y. Moore, S.T. Dekosky. Cognitive correlates of cortical cholinergic denervation in Parkinson's disease and parkinsonian dementia. J. Neurol., 253 (2) (2006 Feb), pp. 242-247, 10.1007/s00415-005-0971-0ISTEX
17. H. Shimada, S. Hirano, H. Shinotoh, A. Aotsuka, K. Sato, N. Tanaka, T. Ota, M. Asahina, K. Fukushi, S. Kuwabara, T. Hattori, T. Suhara, T. Irie. Mapping of brain acetylcholinesterase alterations in Lewy body disease by PET. Neurology, 73 (4) (2009 Jul 28), pp. 273-278, 10.1212/WNL.0b013e3181ab2b58
18. D.E. Kuhl, S. Minoshima, J.A. Fessler, K.A. Frey, N.L. Foster, E.P. Ficaro, D.M. Wieland, R.A. Koeppe. In vivo mapping of cholinergic terminals in normal aging, Alzheimer's disease, and Parkinson's disease. Ann. Neurol., 40 (3) (1996 Sep), pp. 399-410, 10.1002/ana.410400309ISTEX
19. J. Mazère, C. Prunier, O. Barret, M. Guyot, C. Hommet, D. Guilloteau, *et al.* In vivo SPECT imaging of vesicular acetylcholine transporter using [(123)I]-IBVM in early Alzheimer's disease. Neuroimage, 40 (2008), pp. 280-288.

20. J. Mazère, F. Lamare, M. Allard, P. Fernandez, W. Mayo. 123I-Iodobenzovesamicol SPECT imaging of cholinergic systems in dementia with Lewy bodies. J. Nucl. Med., 58 (1) (2017 Jan), pp. 123-128, 10.2967/jnumed.116.176180
21. G.K. Mulholland, D.M. Wieland, M.R. Kilbourn, K.A. Frey, P.S. Sherman, J.E. Carey, D.E. Kuhl. [18F]fluoroethoxy-benzovesamicol, a PET radiotracer for the vesicular acetylcholine transporter and cholinergic synapses. Synapse, 30 (3) (1998 Nov), 10.1002/(SICI)1098-2396(199811)30:3<263::AID-SYN4>3.0.CO;2–9ISTEX 263-74.
22. M.J. Parent, M.A. Bedard, A. Aliaga, L. Minuzzi, N. Mechawar, J.P. Soucy, E. Schirrmacher, A. Kostikov, S.G. Gauthier, P. Rosa-Neto. Cholinergic depletion in alzheimer's disease shown by [(18) F]FEOBV autoradiography. Int. J. Mol. Imaging, 2013 (2013), p. 205045, 10.1155/2013/205045
23. M. Aghourian, C. Legault-Denis, J.P. Soucy, P. Rosa-Neto, S. Gauthier, A. Kostikov, P. Gravel, M.A. Bédard. Quantification of brain cholinergic denervation in Alzheimer's disease using PET imaging with [18F]-FEOBV. Mol Psychiatry, 22 (11) (2017 Nov), pp. 1531-1538, 10.1038/mp.2017.183
24. T.W. Schmitz, M. Mur, M. Aghourian, M.A. Bedard, R.N. Spreng. Alzheimer's disease neuroimaging initiative. Longitudinal alzheimer's degeneration reflects the spatial topography of cholinergic basal forebrain projections. Cell Rep., 24 (1) (2018 Jul 3), pp. 38-46, 10.1016/j.celrep.2018.06.001
25. N.I. Bohnen, P. Kanel, Z. Zhou, R.A. Koeppe, K.A. Frey, W.T. Dauer, R.L. Albin, M.L.T.M. Müller. Cholinergic system changes of falls and freezing of gait in Parkinson's disease. Ann. Neurol., 85 (4) (2019 Apr), pp. 538-549, 10.1002/ana.25430
26. S. van der Zee, M.L.T.M. Müller, P. Kanel, T. van Laar, N.I. Bohnen. Cholinergic denervation patterns across cognitive domains in Parkinson's disease. Mov. Disord. (2020 Nov 2), 10.1002/mds.28360
27. S. Nejad-Davarani, R.A. Koeppe, R.L. Albin, K.A. Frey, M.L.T.M. Müller, N.I. Bohnen. Quantification of brain cholinergic denervation in dementia with Lewy bodies using PET imaging with [18 F]-FEOBV. Mol. Psychiatr., 24 (3) (2019 Mar), pp. 322-327, 10.1038/s41380-018-0130-5
28. P. Kanel, M.L.T.M. Müller, S. van der Zee, C.A. Sanchez-Catasus, R.A. Koeppe, K.A. Frey. Bohnen NI.topography of cholinergic changes in dementia with Lewy bodies and key neural network hubs. J neuropsychiatry clin neurosci, Fall, 32 (4) (2020), pp. 370-375, 10.1176/appi.neuropsych.19070165
29. C. Geula, M.M. Mesulam. Systematic regional variations in the loss of cortical cholinergic fibers in Alzheimer's disease. Cerebr. Cortex, 6 (2) (1996 Mar-Apr), pp. 165-177, 10.1093/cercor/6.2.165ISTEX
30. M.M. Mesulam. The systems-level organization of cholinergic innervation in the human cerebral cortex and its alterations in Alzheimer's disease. Prog. Brain Res., 109 (1996), pp. 285-297, 10.1016/s0079-6123(08)62112-3
31. J.D. Erickson, H. Varoqui, M.K. Schäfer, W. Modi, M.F. Diebler, E. Weihe, J. Rand, L.E. Eiden, T.I. Bonner, T.B. Usdin. Functional identification of a vesicular acetylcholine transporter and its expression from a "cholinergic" gene locus. J. Biol. Chem., 269 (35) (1994 Sep 2), pp. 21929-21932.
32. M.K. Schafer, E. Weihe, J.D. Erickson, L.E. Eiden. Human and monkey cholinergic neurons visualized in paraffin-embedded tissues by immunoreactivity for VAChT, the vesicular acetylcholine transporter. J. Mol. Neurosci., 6 (4) (1995), pp. 225-235, 10.1007/BF02736782ISTEX
33. V.W. Pike. Considerations in the development of reversibly binding PET radioligands for brain imaging. Curr. Med. Chem., 23 (18) (2016), pp. 1818-1869, 10.2174/0929867323666160418114826
34. M. Kovac, S. Mavel, W. Deuther-Conrad, N. Méheux, J. Glöckner, B. Wenzel, M. Anderluh, P. Brust, D. Guilloteau, P. Emond. 3D QSAR study, synthesis, and in vitro evaluation of (+)-5-FBVM as potential PET radioligand for the vesicular acetylcholine transporter (VAChT). Bioorg. Med. Chem., 18 (21) (2010 Nov 1), pp. 7659-7667, 10.1016/j.bmc.2010.08.028ISTEX
35. X. Deng, J. Rong, L. Wang, N. Vasdev, L. Zhang, L. Josephson, S.H. Liang. Chemistry for positron emission tomography: recent advances in 11C-18F-, 13N-, and 15O-Labeling Reactions. Angew Chem Int Ed Engl, 58 (9) (2019 Feb 25), pp. 2580-2605, 10.1002/anie.201805501
36. M. Tredwell, S.M. Preshlock, N.J. Taylor, S. Gruber, M. Huiban, J. Passchier, J. Mercier, C. Génicot, V. Gouverneur. A general copper-mediated nucleophilic 18F fluorination of arenes. Angew Chem Int (Ed.), Englera, 53 (30) (2014 Jul 21), pp. 7751-7755, 10.1002/anie.201404436ISTEX
37. P.W. Miller, N.J. Long, R. Vilar, A.D. Gee. Synthesis of 11C, 18F, 15O, and 13N radiolabels for positron emission tomography. Angew. Chem. Int. Ed., 47 (2008), pp. 8998-9033.
38. J. Elie, J. Vercouillie, N. Arlicot, L. Lemaire, R. Bidault, S. Bodard, C. Hosselet, J.B. Deloye, S. Chalon, P. Emond, D. Guilloteau, F. Buron, S. Routier. Design of selective COX-2 inhibitors in the (aza)indazole series. Chemistry, in vitro studies, radiochemistry and evaluations in rats of a [18F] PET tracer. J. Enzym. Inhib. Med. Chem., 34 (1) (2019 Dec), pp. 1-7, 10.1080/14756366.2018.1501043
39. S.M.N. Efange, A.B. Khare, K. von Hohenberg, R.H. Mach, S.M. Parsons, Z. Tu. Synthesis and in vitro biological evaluation of carbonyl group-containing inhibitors of vesicular acetylcholine transporter. J. Med. Chem., 53 (7) (2010 Apr 8), pp. 2825-2835, 10.1021/jm9017916
40. B. Xing, C. Ni, J. Hu. Hypervalent iodine(III)-Catalyzed balz–schiemann fluorination under mild conditions. Angew chem int, Englera, 57 (31) (2018 Jul 26), pp. 9896-9900, 10.1002/anie.201802466
41. R.W.W. Hooft, L.H. Straver, A.L. Spek. Determination of absolute structure using Bayesian statistics on Bijvoet differences. J. Appl. Crystallogr., 41 (Pt 1) (2008 Feb 1), pp. 96-103, 10.1107/S0021889807059870ISTEX

42. H.D. Flack, G. Bernardinelli. Absolute structure and absolute configuration. Acta Crystallogr. A, 55 (Pt 5) (1999 Sep 1), pp. 908-915, 10.1107/s0108767399004262ISTEX
43. S. Parsons, H.D. Flack, T. Wagner. Use of intensity quotients and differences in absolute structure refinement. Acta Crystallogr B Struct Sci Cryst Eng Mater, 69 (Pt 3) (2013 Jun), pp. 249-259, 10.1107/S2052519213010014
44. G.K. Mulholland, Y.-W. Jung, D.M. Wieland, M.R. Kilbourn, D.E. Kuhl. Synthesis of [18F]fluoroethoxy-benzovesamicol, a radiotracer for cholinergic neurons. J. Label. Compd. Radiopharm., 33 (1993), pp. 583-591.
45. G.A. Rogers, S.M. Parsons, D.C. Anderson, L.M. Nilsson, B.A. Bahr, W.D. Kornreich, R. Kaufman, R.S. Jacobs, B. Kirtman. Synthesis, in vitro acetylcholine-storage-blocking activities, and biological properties of derivatives and analogues of trans-2-(4-phenylpiperidino)cyclohexanol (vesamicol). J. Med. Chem., 32 (6) (1989 Jun), pp. 1217-1230, 10.1021/jm00126a013ISTEX
46. Y.W. Jung, K.A. Frey, G.K. Mulholland, R. del Rosario, P.S. Sherman, D.M. Raffel, M.E. Van Dort, D.E. Kuhl, D.L. Gildersleeve, D.M. Wieland. Vesamicol receptor mapping of brain cholinergic neurons with radioiodine-labeled positional isomers of benzovesamicol. J. Med. Chem., 39 (17) (1996 Aug 16), pp. 3331-3342, 10.1021/jm9507486ISTEX
47. M. Scheunemann, D. Sorger, B. Wenzel, K. Heinitz, R. Schliebs, M. Klingner, *et al.* Synthesis of novel 4- and 5-substituted benzyl ether derivatives of vesamicol and in vitro evaluation of their binding properties to the vesicular acetylcholine transporter site. Bioorg. Med. Chem., 12 (6) (2004 Mar 15), pp. 1459-1465, 10.1016/j.bmc.2003.12.035ISTEX
48. Y. Cheng, W.H. Prusoff. Relationship between the inhibition constant (K1) and the concentration of inhibitor which causes 50 percent inhibition (I50) of an enzymatic reaction. Biochem. Pharmacol., 22 (23) (1973 Dec 1), pp. 3099-3108, 10.1016/0006-2952(73)90196-2ISTEX
49. M.R. Kilbourn, B. Hockley, L. Lee, P. Sherman, C. Quesada, K.A. Frey, R.A. Koeppe. Positron emission tomography imaging of (2R,3R)-5-[(18)F]fluoroethoxybenzovesamicol in rat and monkey brain: a radioligand for the vesicular acetylcholine transporter. Nucl. Med. Biol., 36 (5) (2009 Jul), pp. 489-493, 10.1016/j.nucmedbio.2009.02.007ISTEX
50. M. Parent, M.A. Bedard, A. Aliaga, J.P. Soucy. Landry st-pierre E, cyr M, kostikov A, schirrmacher E, massarweh G, rosa-neto P. PET imaging of cholinergic deficits in rats using [18F]fluoroethoxybenzovesamicol ([18F]FEOBV). Neuroimage, 62 (1) (2012 Aug 1), pp. 555-561, 10.1016/j.neuroimage.2012.04.032ISTEX
51. M. Cyr, M.J. Parent, N. Mechawar, P. Rosa-Neto, J.P. Soucy, S.D. Clark, M. Aghourian, M.A. Bedard. Deficit in sustained attention following selective cholinergic lesion of the pedunculopontine tegmental nucleus in rat, as measured with both post-mortem immunocytochemistry and in vivo PET imaging with [^{18}F]fluoroethoxybenzovesamicol. Behav. Brain Res., 278 (2015 Feb 1), pp. 107-114, 10.1016/j.bbr.2014.09.021
52. A. Schildt, E.F.J. de Vries, A.T.M. Willemsen, B.L. Giacobbo, R. Moraga-Amaro, J.W.A. Sijbesma, A. van Waarde, V. Sossi, R.A.J.O. Dierckx, J. Doorduin. Effect of dopamine D2 receptor antagonists on [18F]-FEOBV binding. Mol. Pharm., 17 (3) (2020 Mar 2), pp. 865-872, 10.1021/acs.molpharmaceut.9b01129
53. J.M. Cisneros-Franco, P. Voss, M.S. Kang, M.E. Thomas, J. Côté, K. Ross, P. Gaudreau, D.A. Rudko, P. Rosa-Neto, É. de-Villers-Sidani. PET imaging of perceptual learning-induced changes in the aged rodent cholinergic system. Front. Neurosci., 13 (2020 Jan 21), p. 1438, 10.3389/fnins.2019.01438
54. M. Petrou, K.A. Frey, M.R. Kilbourn, P.J. Scott, D.M. Raffel, N.I. Bohnen, M.L. Müller, R.L. Albin, R.A. Koeppe. In vivo imaging of human cholinergic nerve terminals with (-)-5-(18)F-fluoroethoxybenzovesamicol: biodistribution, dosimetry, and tracer kinetic analyses. J. Nucl. Med., 55 (3) (2014 Mar), pp. 396-404, 10.2967/jnumed.113.124792
55. T.W. Schmitz, M. Mur, M. Aghourian, M.A. Bedard, R.N. Spreng. Alzheimer's disease neuroimaging initiative. Longitudinal alzheimer's degeneration reflects the spatial topography of cholinergic basal forebrain projections. Cell Rep., 24 (1) (2018 Jul 3), pp. 38-46, 10.1016/j.celrep.2018.06.001
56. S. Nejad-Davarani, R.A. Koeppe, R.L. Albin, K.A. Frey, M.L.T.M. Müller, N.I. Bohnen. Quantification of brain cholinergic denervation in dementia with Lewy bodies using PET imaging with [18F]-FEOBV. Mol. Psychiatr., 24 (3) (2019 Mar), pp. 322-327, 10.1038/s41380-018-0130-5
57. N.I. Bohnen, P. Kanel, Z. Zhou, R.A. Koeppe, K.A. Frey, W.T. Dauer, R.L. Albin, M.L.T.M. Müller. Cholinergic system changes of falls and freezing of gait in Parkinson's disease. Ann. Neurol., 85 (4) (2019 Apr), pp. 538-549, 10.1002/ana.25430
58. P. Kanel, M.L.T.M. Müller, S. van der Zee, C.A. Sanchez-Catasus, R.A. Koeppe, K.A. Frey, N.I. Bohnen. Topography of cholinergic changes in dementia with Lewy bodies and key neural network hubs. J neuropsychiatry clin neurosci, Fall, 32 (4) (2020), pp. 370-375, 10.1176/appi.neuropsych.19070165
59. C. Sanchez-Catasus, N.I. Bohnen, N. D'Cruz, M. Muller. Striatal acetylcholine-dopamine imbalance in Parkinson's disease: in vivo neuroimaging study with dual-tracer PET and dopaminergic PET-informed correlational tractography. J. Nucl. Med. (2021 Jul 16), 10.2967/jnumed.121.261939
60. M. Aghourian. Aumont É, Grothe MJ, Soucy JP, Rosa-Neto P, Bedard MA. FEOBV-PET to quantify cortical cholinergic denervation in AD: relationship to basal forebrain volumetry. J. Neuroimaging, 31 (6) (2021 Nov), pp. 1077-1081, 10.1111/jon.12921
61. C. Legault-Denis, M. Aghourian, J.P. Soucy, P. Rosa-Neto, A. Dagher, E. Aumont, R. Wickens, M.A. Bedard. Normal cognition in Parkinson's disease may involve hippocampal cholinergic compensation: an exploratory PET imaging study with [(18)F]-FEOBV. Park. Relat. Disord., 91 (2021 Oct), pp. 162-166, 10.1016/j.parkreldis.2021.09.018

62. C. Barthel, D. Sorger, W. Deuther-Conrad, M. Scheunemann, S. Schweiger, P. Jackel, *et al.* New systematically modified vesamicol analogs and their affinity and selectivity for the vesicular acetylcholine transporter - a critical examination of the lead structure. Eur. J. Med. Chem., 100 (2015 Jul 15), pp. 50-67, 10.1016/j.ejmech.2015.05.033
63. W.D. Bowen, E.L. Moses, P.J. Tolentino, J.M. Walker. Metabolites of haloperidol display preferential activity at sigma receptors compared to dopamine D-2 receptors. Eur. J. Pharmacol., 177 (3) (1990 Feb 27), pp. 111-118, 10.1016/0014-2999(90)90260-dISTEX
64. M. Ingvar, S. Stone-Elander, G.A. Rogers, B. Johansson, L. Eriksson, S.M. Parsons, L. Widén. Striatal D2/acetylcholine interactions: PET studies of the vesamicol receptor. Neuroreport, 4 (12) (1993 Sep 30), pp. 1311-1314.
65. S.M. Efange, R.B. Langason, A.B. Khare. Age-related diminution of dopamine antagonist-stimulated vesamicol receptor binding. J. Nucl. Med., 37 (7) (1996 Jul), pp. 1192-1197.
66. D.J. McCann, A.D. Weissman, T.P. Su. Sigma-1 and sigma-2 sites in rat brain: comparison of regional, ontogenetic, and subcellular patterns. Synapse, 17 (3) (1994 Jul), pp. 182-189, 10.1002/syn.890170307ISTEX
67. G. Sheldrick. Crystal structure refinement with SHELXL. Acta Crystallogr. C, 71 (2015), pp. 3-8.
68. O.V. Dolomanov, L.J. Bourhis, R.J. Gildea, J.A.K. Howard, H. Puschmann. OLEX2: a complete structure solution, refinement and analysis program. J. Appl. Crystallogr., 42 (2009), pp. 339-341.